Electronic Supplementary Material (ESI) for Nanoscale.

Supporting information

Seeing the Diabetes: Visual Detection of Glucose Based on the Intrinsic Peroxidase-Like Activity of MoS_2 Nanosheets

Tianran Lin, Liangshuang Zhong, Liangqia Guo, Fengfu Fu and Guonan Chen*

Ministry of Education Key Laboratory of Analysis and Detection for Food Safety, Fujian Provincial Key Laboratory of Analysis and Detection Technology for Food Safety, and Department of Chemistry, Fuzhou University, Fuzhou, Fujian, 350108, China. Fax: +86 591-22866135; Tel: +86 591-22866135; E-mail: lqguo@fzu.edu.cn

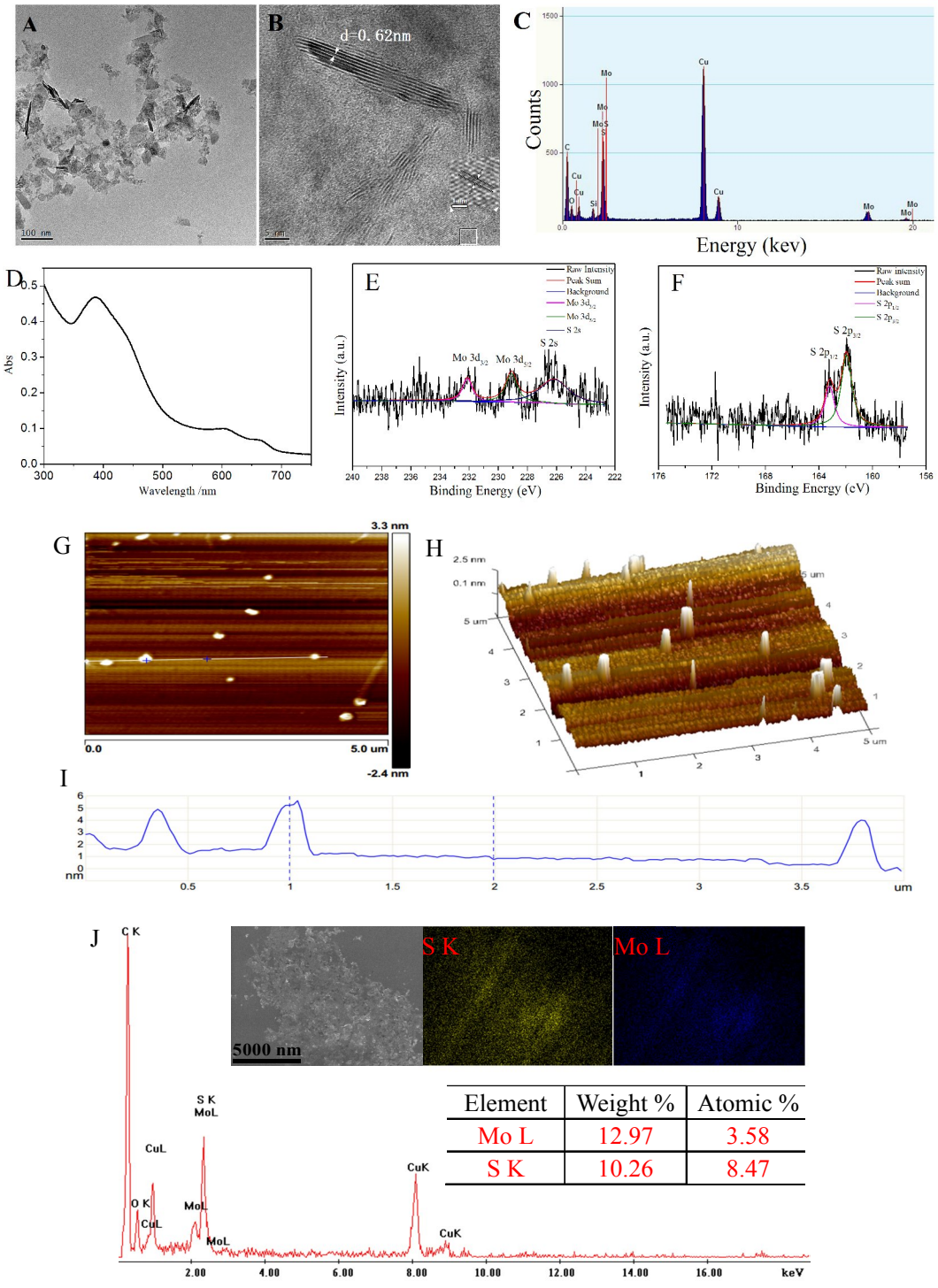

Element	Weight %	Atomic %
Mo L	12.97	3.58
S K	10.26	8.47

Fig.S1. TEM image (A), HRTEM image (B), TEM-based EDX pattern (C), UV-vis absorption spectrum (1.8 μg mL^{-1} MoS_2 nanosheets) (D), XPS Mo 3d core-level spectrum (E), XPS S 2p core-level spectrum (F), AFM image (G), AFM 3D height profile (H), height profile along the white line shown in the AFM image (I), SEM-based EDX pattern (Inset are SEM image, S and Mo mapping images) (J) of MoS_2 nanosheets before catalysis reaction. The signals of Cu, C and O in TEM-based EDX and SEM-based EDX patterns (C, J) originated from the carbon film supported by copper grids.

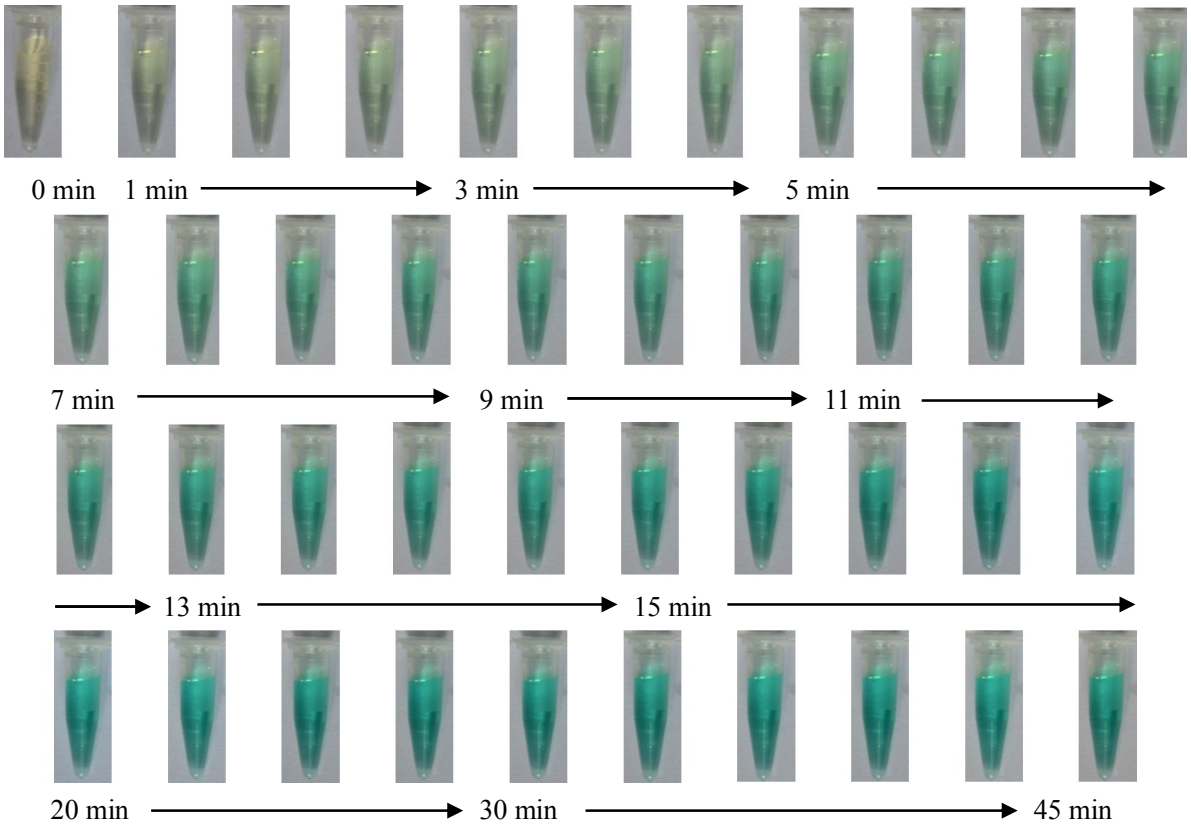

Fig.S2. The color changing with the increasing of reaction time after mixing MoS_2 nanosheets (1.8 μg mL^{-1}) with TMB (1.2 mmol L^{-1}) and H_2O_2 (0.04 mmol L^{-1}) in a reaction volume of 0.5 mL Tris-HCl buffer (10 mmol L^{-1}, pH 6.9)

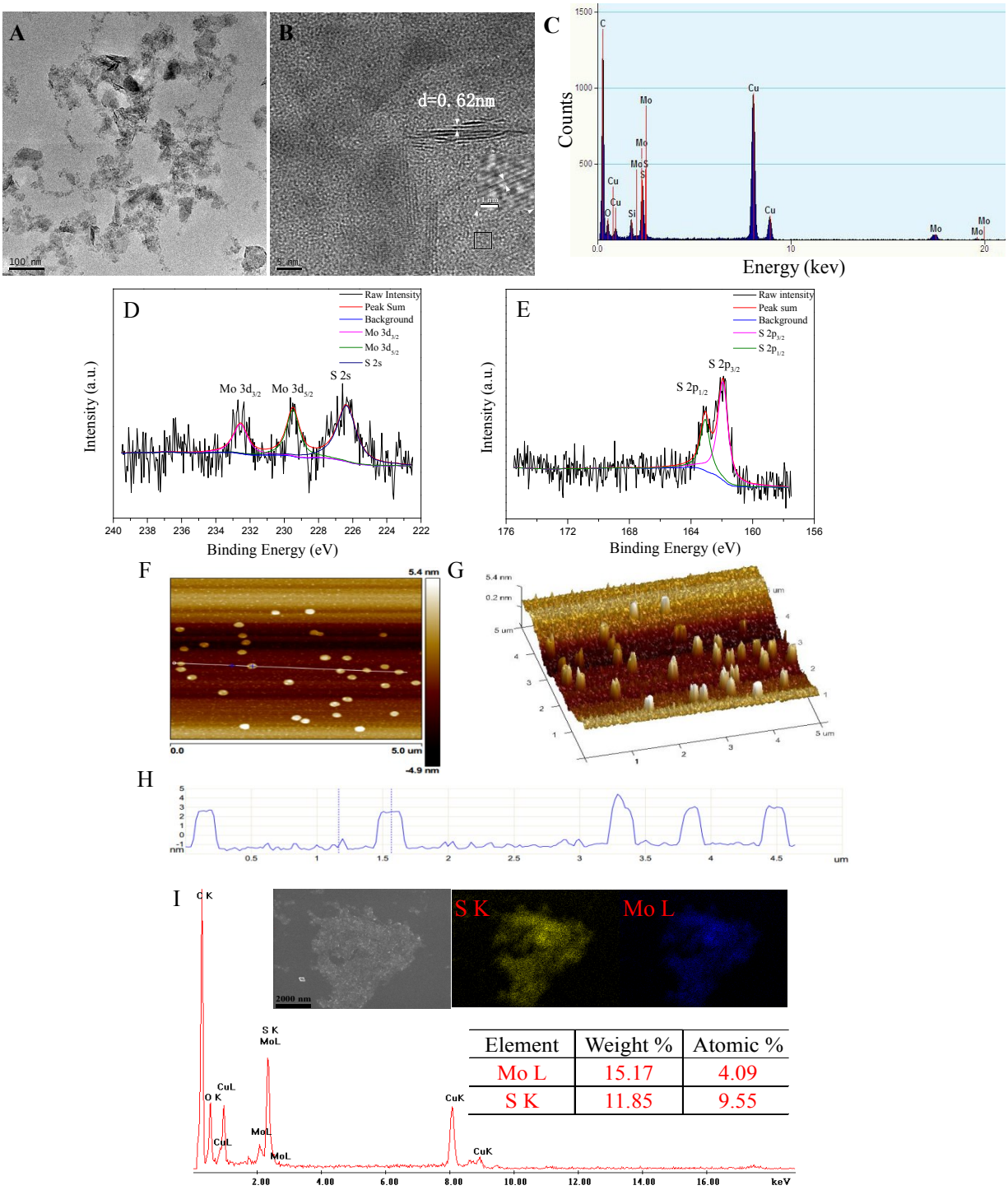

Fig.S3. TEM image (A), HRTEM image (B), TEM-based EDX pattern (C), XPS Mo 3d core-level spectrum (D), XPS S 2p core-level spectrum (E), AFM image (F), AFM 3D height profile (G), height profile along the white line shown in the AFM image (H), SEM-based EDX pattern (Inset are SEM image, S and Mo mapping images) (I) of MoS_2 nanosheets after catalysis reaction. The signals of Cu, C and O in TEM-based EDX and SEM-based EDX patterns (C, I) originated from the carbon film supported by copper grids.

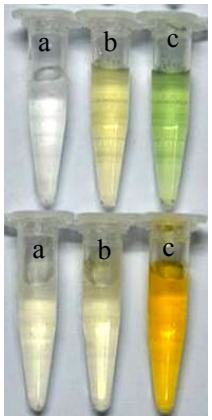

Fig.S4. Photos of oxidation reaction of ABTS (20 mmol L^{-1}) in Tris-HCl buffer (pH 7.0, 10 mmol L^{-1}) (A) and OPD (300 mmol L^{-1}) in HAc-NaAc buffer (pH 4.0, 200 mmol L^{-1}) (B) in the presence of H_2O_2 (0.04 mmol L^{-1}) (a), MoS_2 (1.8 μg mL^{-1}) (b), and H_2O_2 (0.04 mmol L^{-1}) + MoS_2 (1.8 μg mL^{-1}) (c) at room temperature after reaction for 12 min.

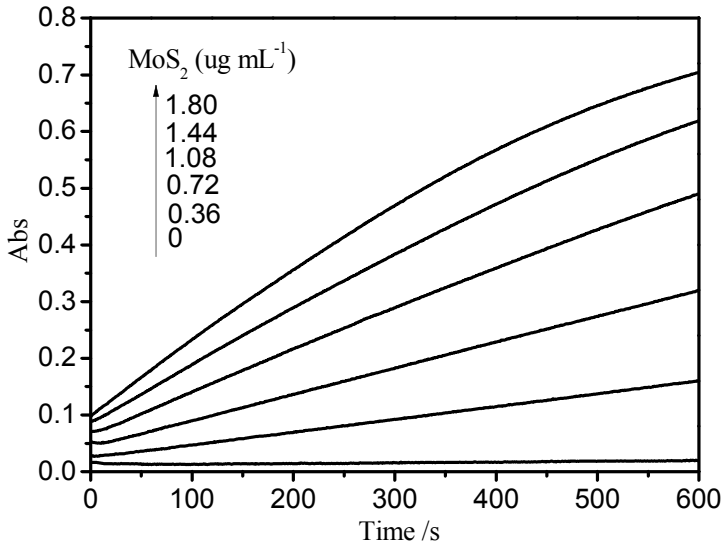

Fig.S5. The time-dependent absorbance changes at 652 nm in the presence of different concentrations of MoS_2 nanosheets in Tris-HCl buffer (10 mmol L^{-1}, pH 6.9) at 30 °C.

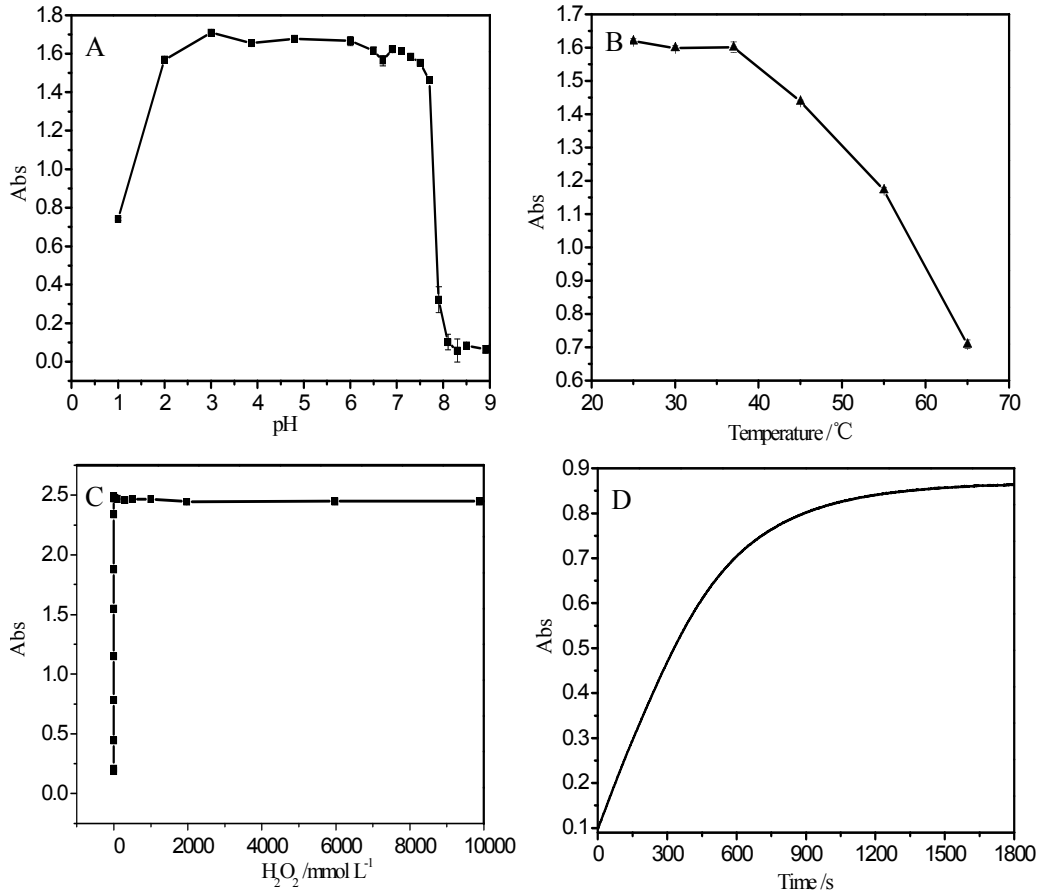

Fig.S6. Effect of pH (A), temperature (B), H_2O_2 concentration (C), and reaction time (D) on the peroxidase-like activity of MoS_2 nanosheets for the TMB oxidation. The experiment was carried out using 1.8 μg mL^{-1} MoS_2 nanosheets in a reaction volume of 0.5 mL, in Tris-HCl buffer (10 mmol L^{-1}, pH 6.9) with 1.2 mmol L^{-1} TMB and 0.04 mmol L^{-1} H_2O_2 for 30 min at 30 °C. The error bars represent the standard deviation of three measurements.

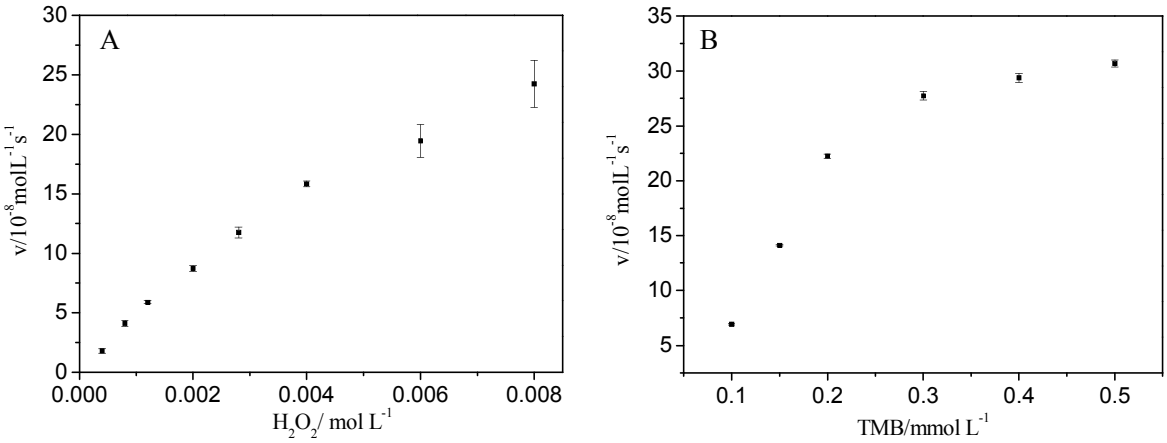

Fig.S7. Steady-state kinetic assay of HRP. The velocity (v) of the reaction was measured using HRP (5 ng L^{-1}) in 0.5 mL Tris-HCl buffer (10 mmol L^{-1}, pH 6.9) at 30℃. (A) The concentration of TMB was 1.2 mmol L^{-1} and H_2O_2 concentration was varied. (B) The concentration of H_2O_2 was 3.2 mmol L^{-1} and TMB concentration was varied.

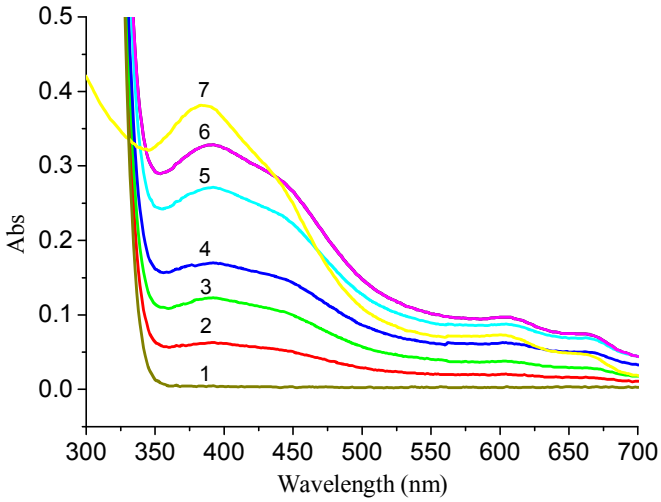

Fig.S8. Absorption spectra of TMB (1), MoS_2 nanosheets (7), and a fixed concentration of TMB interacting with different concentrations of MoS_2 nanosheets (2-6)

(1) 50 μL TMB (12 mmol L^{-1}) + 50 μL H_2O + 200 μL Tris-HCl (pH 6.9, 10 mmol L^{-1}) + 200 μL H_2O

(2) 50 μL TMB (12 mmol L^{-1}) + 10μL MoS_2 (18 μg mL^{-1}) + 40 μL H_2O + 200 μL Tris-HCl (pH6.9, 10 mmol L^{-1}) + 200 μL H_2O

(3) 50 μL TMB (12 mmol L^{-1}) + 20 μL MoS_2 (18μg mL^{-1}) + 30 μL H_2O + 200 μL Tris-HCl (pH6.9, 10 mmol L^{-1}) + 200 μL H_2O

(4) 50 μL TMB (12 mmol L^{-1}) + 30 μL MoS_2 (18 μg mL^{-1}) + 20 μL H_2O + 200 μL Tris-HCl (pH6.9, 10 mmol L^{-1}) + 200 μL H_2O

(5) 50 μL TMB (12 mmol L^{-1}) + 40 μL MoS_2 (18 μg mL^{-1}) + 10 μL H_2O + 200 μL Tris-HCl (pH6.9, 10 mmol L^{-1}) + 200 μL H_2O

(6) 50 μL TMB (12 mmol L^{-1}) + 50 μL MoS_2 (18 μg mL^{-1}) + 200 μL Tris-HCl (pH6.9, 10 mmol L^{-1}) + 200 μL H_2O

(7) 50 μL H_2O + 50 μL MoS_2 (18 μg mL^{-1}) + 200 μL Tris-HCl (pH6.9,10 mmol L^{-1}) + 200 μL H_2O

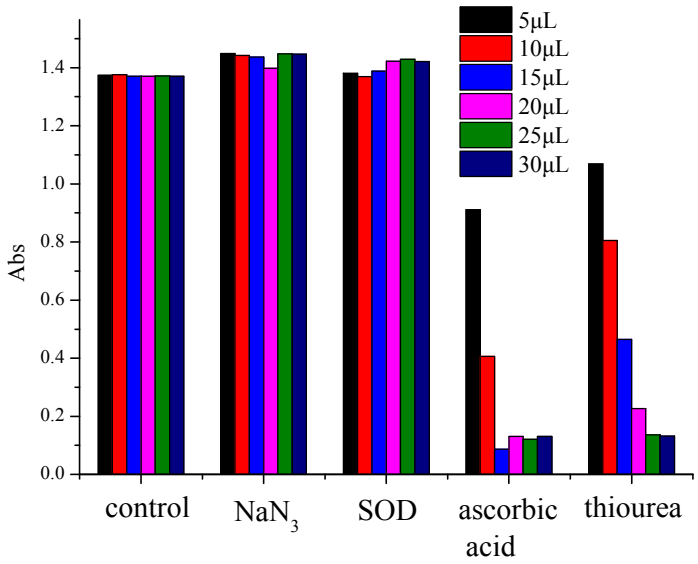

Fig.S9. The catalytic reaction at the presence of different radical scavengers

Procedures: 50 μL MoS_2 (18 μg mL^{-1}), 200 μL Tris-HCl (6.9, 10 mmol L^{-1}), 50 μL TMB (12 mmol L^{-1}) and different volumes of radical scavenger were mixed. The volume of the mixture was adjusted to 400 μL with water, then 200 μL H_2O_2 (0.1 mmol L^{-1}) was added. After the reaction was carried out at room temperature for 30 min, 20 μL H_2SO_4 (v/v:20%) was added into the above mixture. The absorbance at 450 nm was recorded. The original concentrations of NaN_3, ascorbic acid, thiourea and SOD were 1 mmol L^{-1}, 1 mmol L^{-1}, 1 mmol L^{-} and 20 U mL^{-1}, respectively.

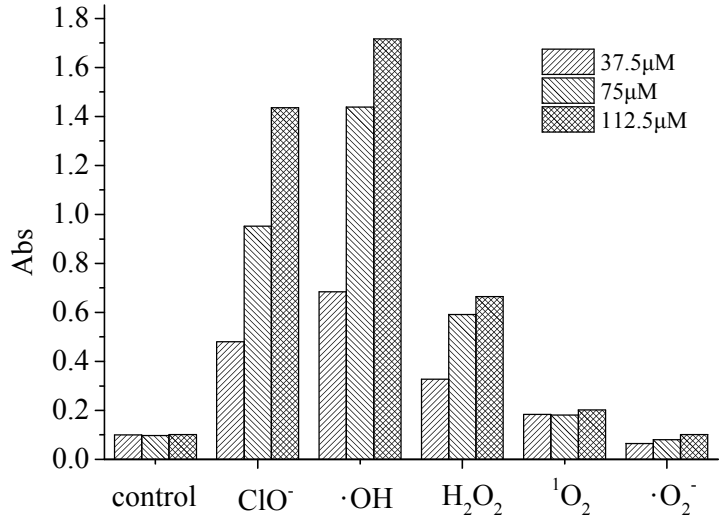

Fig. S10. The response of this catalytic reaction to various ROS
Procedures: 50 μL MoS_2 (18 μg mL^{-1}), 200 μL Tris-HCl (6.9, 10 mmol L^{-1}), 50 μL TMB (12 mmol L^{-1}) and 200 μL ROS were mixed. After the reaction was carried out at room temperature for 30 min. The absorbance at 652 nm was recorded.

The generation of ROS was performed using documented protocols (Abo et al. 2011 J. Am. Chem. Soc. 133, 10629-10637; Chen et al. 2013 J. Am. Chem. Soc. 135, 11595-11602; Lee et al. 2009 Adv. Funct. Mater. 19(12), 1884-1890). Hydroxyl radical (·OH) was generated by the Fenton reaction between H_2O_2 and ferrous sulphate at a molar concentration ratio of 10:1. Hypochlorite (ClO^-) and superoxide anion ($O_2{\cdot}^-$) were obtained from NaOCl and KO_2, respectively. The singlet oxygen ($^1O_2$) was produced by H_2O_2 with NaClO. The absorbance was enhanced greatly at the presence of ·OH, ClO^- as well as H_2O_2.

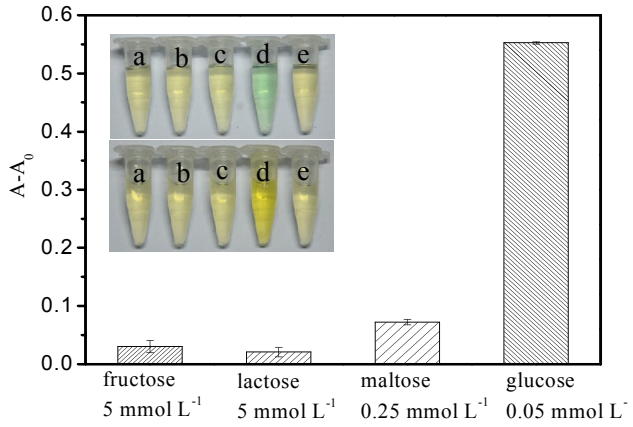

Fig.S11. Selectivity analysis for glucose detection by monitoring the relative absorbance. Inset of Fig.S9 were images of colored production for the different solutions ((a) 5 mmol L^{-1} fructose, (b) 5 mmol L^{-1} lactose, (c) 0.25 mmol L^{-1} maltose, (d) 0.05 mmol L^{-1} glucose, and blank). The error bars represent the standard deviation of three measurements.

Table S1. Comparison of the apparent Michaelies-Menten constant (K_m) and maximum reaction rate (V_{max}) between MoS_2 and HRP. K_m is the Michaelies constant, V_{max} is the maximal reaction velocity.

Catalyst	substance	K_m (mmol L^{-1})	V_{max} (mol L^{-1}/s)
MoS_2	H_2O_2	0.0116	4.29×10^{-8}
MoS_2	TMB	0.525	5.16×10^{-8}
HRP	H_2O_2	10.9	58.5×10^{-8}
HRP	TMB	0.172	41.8×10^{-8}

Table S2. Results of determination of glucose in serum samples

	Glucose meter method [a] (mmol L^{-1})	Proposed method [b] (mmol L^{-1})	RSD (%)
Serum 1	5.00	4.53 ± 0.02 [c]	-9.4%
Serum 2	6.67	6.31 ± 0.01 [c]	-5.4%
Serum 3	8.33	7.79 ± 0.01 [c]	-6.5%

[a] The glucose determination was performed by the conventional enzymatic method at the First Affiliated Hospital of Fujian Medical University.

[b] The confidence level was 95%.

[c] n=3